ELSEVIER

Earth and Planetary Science Letters 145 (1996) 109–123

EPSL

Modelling plume-related uplift, gravity and melting on Venus

Francis Nimmo *, Dan McKenzie [1]

Institute of Theoretical Geophysics, Bullard Laboratories, Madingley Road, Cambridge, CB3 0EZ, UK

Received 15 April 1996; revised 8 October 1996; accepted 10 October 1996

Abstract

Three roughly circular regions on Venus about 1000 km across are identified as potential Hawaii-scale plume sites on the basis of their gravity (70–90 mgal) and topography (1.6–2.0 km) anomalies, and signs of melt generation and rifting. Axisymmetric isoviscous convection models are used to reproduce gravity profiles across these plumes and the line-of-sight acceleration of the Magellan spacecraft as it passes over them. The best fitting models have a conductive lid thickness of less than 150 km, mantle viscosity of 8.9×10^{19} to 9.6×10^{20} Pa s and a basal heat flux of 15–25 m W m^{-2}. The lid thickness is constrained by requiring a modest amount of melt generation and a potential temperature of about 1300°C. The high mantle viscosity relative to that of Earth is probably a consequence of the absence of water in the mantle, and may help to explain the current absence of plate tectonics on Venus. The low heat flux suggests that the thermal evolution of Venus has differed from that of the Earth.

Keywords: gravity anomalies; heat flow; hot spots; lithosphere; Magellan Program; Venus; mantle; convection; models; topography; viscosity; volcanism

1. Introduction

Areas overlying terrestrial mantle plumes are usually characterized by positive gravity and topography anomalies, melt generation and extension [1]. On the basis of gravity, topography and synthetic aperture radar (SAR) images, at least ten areas on Venus have been identified as possible plume sites [2–7], and may therefore provide important information about the state of the Venusian mantle. The largest of these regional rises, Beta Regio, has a maximum gravity anomaly of 220 mgal and a diameter of 2500 km [8]. In contrast, Hawaii, the most vigorously convecting plume beneath terrestrial oceanic lithosphere, shows a long wavelength gravity anomaly of about 50 mgal and a diameter of 1500 km [9]. This paper uses data from several possible plumes on Venus which have a scale similar to that of Hawaii to place constraints on the thermal structure of the mantle, based on convective models of these plumes. Section 2 is concerned with the identification of these plume sites, and the constraints they place on the convective models, whilst Section 3 describes the modelling. Section 4 examines how the models relate to the observations and Section 5 discusses the implications of the best-fitting models.

* Corresponding author. E-mail: nimmo@esc.cam.ac.uk

[1] E-mail: mckenzie@esc.cam.ac.uk.

PII S0012-821X(96)00200-2

2. Observational constraints

The gravity field of Venus has been described by spherical harmonics to degree and order 90, which is equivalent to a wavelength of 420 km. Estimates of the elastic thickness of the lithosphere vary from about 10 km to 50 km from spectral studies [8,10–12] and examinations of topographic flexure [13,14], which implies that any gravity signal at wavelengths longer than about 1000 km cannot be due to elastic effects. With wavelengths shorter than about 1000 km filtered out, maps of Venus gravity show circular positive and more sheet-like negative gravity anomalies [8,15], which are the patterns expected for vigorous convection. Moreover, the admittance of these long wavelength signals is about 50 mgal/km, similar to values obtained in high Rayleigh number convective models with constant viscosity and a lid thickness of around 70 km ([8], table 1). Therefore, any roughly circular region 1000 km or more across having positive gravity and topography anomalies is a potential active plume site, especially if it shows signs of melt generation and rifting.

The Rayleigh number of convection within the mantle of Venus is likely to be at least $\sim 10^6$. The circulation is therefore likely to be strongly time dependent, with rising and sinking plumes superimposed on a larger scale planform that is also time dependent. The number and location of plumes in such a circulation will depend on what criteria are used to define such features. These expectations suggest that the largest convective plumes on Venus will be hard to model, since they will involve large-scale flow with thin thermal boundary layers. Since the effects of a plume with a 100 km wavelength would not be visible at the top of a 200 km thick lithosphere, the smallest scale of convective feature visible at the surface provides an upper bound on the lithospheric thickness. We therefore chose to study smaller convective features. A convective model must be capable of reproducing the smaller as well as the larger features.

Stofan et al. [7] identified nine probable sites of mantle upwelling on Venus and there may be others (e.g., Ulfrun Regio [5]). These sites show regional topographic rises of 0.5–2.5 km, diameters of 1000–2500 km [7] and gravity anomalies of 50–220 mgal. They are generally more extensive and have larger amplitude gravity and topography anomalies than does Hawaii.

One of the areas identified in [7] has been selected as a Hawaii-scale feature having a gravity profile which looks similar in shape to theoretical profiles. The gravity anomaly, Δg, of the site is obtained by using the $l = m = 90$ spherical harmonic gravity (MGNP90LSAAP; W. Sjogren, pers. commun.) to compare the maximum value at the plume site with that of the surrounding plains. The topography anomaly, Δh, is obtained in a similar manner using an $l = m = 75$ spherical harmonic topography expansion. This site is centred at Bell, 30°N, 48°E, the geology and gravity of which are described in detail elsewhere [10,16]. The Magellan SAR picture (C1-MIDR) 30N045 shows flows radiating outwards at least 700 km, overprinting areas of tessera and wrinkle ridges. The main volcanic centre, Tepev Mons, produces radar-dark flows; F-MIDR 30N047 shows that this centre possesses a radial array of linked circular pits, individual pits being up to 5 km across. A second collection of three volcanic edifices, up to 30 km in diameter, which produce flows that are more radar-bright, is found 300 km west of this centre. The gravity anomaly, Δg, is about 80 mgal and the topography anomaly, Δh, is 2.0 km, although the presence of the volcanic constructs makes it difficult to assess the maximum amplitude of the regional swell. Smrekar [10] finds an elastic thickness of 25–35 km from admittance studies at wavelengths of 500–800 km.

Two other plumes were used that were not listed in [7]. That east of Eistla Regio at 0°N, 34°E will be referred to as Farida, a nearby impact crater, to avoid confusion with Eastern Eistla, as defined in [7]. Volcanism is more restricted here, the flows not extending more than about 250 km and not showing any signs of being overprinted. The central volcanic edifice shows up on both the topography (Fig. 4d) and F-MIDR 00N037 as an elevated circular area about 100 km across. Δg is 70 mgal and Δh about 1.6 km. The third site is centred at 17°S, 51°W and will be referred to as Eastern Phoebe. The region consists of a circular positive gravity and topography anomaly about 1000 km across, with Δg about 90 mgal and Δh about 1.8 km. C1-MIDRs 15S317 and 15S300 show flows extending at least 500 km to the east and west of the centre, which appears to be

heavily fractured. The fractures mainly post-date the flows, and there is a 300 km diameter double-ring corona 300 km south of the centre. All three of the sites selected have a width at half maximum height of about 500 km.

In order to dimensionalize convective models of these features (see Section 3) we need to specify two of: mantle potential temperature, lithospheric thickness and heat flux, so it is important to investigate how well these quantities are constrained. The surface temperature of Venus is about 450°C but the mantle potential temperature is poorly known. The strongest constraint comes from the basaltic composition of the surface rocks. TiO_2 and K_2O concentrations from the Venera 14 sample suggest that it was formed by decompression melting of a garnet–peridotite source, at a potential temperature of about 1330°C and not higher than 1500°C [17].

The lithospheric thickness is again poorly known, although it is unlikely to be less than the elastic thickness. Melt generation is strongly influenced by lithospheric thickness, however, and the observed uniform impact crater distribution provides some constraints on the time-averaged melt generation rate.

This uniformity is the result of either a global resurfacing event at about 300–500 Ma followed by minor subsequent activity [18,19], or a more gradual resurfacing process [20]. A total surface melt generation rate of about 2 $km^3\ a^{-1}$ is enough to cover the entire surface to a depth of 2 km over 500 Ma, and is sufficient to bury almost all craters [21]. Since fewer than 10% of craters appear to be volcanically embayed from the outside [19,22], the maximum area of the planet likely to have been resurfaced since the hypothetical global event is 20% [23]. Thus the global average rate of generation of melt reaching the surface over the last 300–500 Ma must not exceed 0.4 $km^3\ a^{-1}$. On Earth, surface volcanism is only one half to one tenth of the total volume produced (e.g. [24]). Given that there are probably at least ten Hawaii-scale and larger plumes operating on Venus, the time-averaged melt generation rate of individual Hawaii-scale plumes on Venus probably does not exceed about 0.4 $km^3\ a^{-1}$ (13 $m^3\ s^{-1}$).

Finally, the surface heat flux is unknown, although on the assumption that the heat loss per unit mass on Venus is identical to that on Earth, Solomon and Head obtained a surface heat flux for Venus of 74 mW m^{-2} [25]. The radiogenic heat generation rate is probably similar, given that cosmochemical arguments suggest that U and Th concentrations on Venus should be similar to those of Earth [26] and the K/U ratio measured by the Venera and Vega landers is also similar [27], and different from chondritic meteorites. However, there is no reason why the heat generation rate should equal the heat loss, and the amount of heat produced by the initial planetary accretion is unknown.

3. Theory

The model used employs an axisymmetric geometry and takes an incompressible, Boussinesq fluid with a constant newtonian viscosity and infinite Prandtl number heated entirely from below. It is described in more detail in Watson and McKenzie (hereafter referred to as W&M) [28]. The fluid is contained within a box with stress-free boundary conditions and is overlain by a lid in which heat transfer is entirely conductive. Both temperature and heat flow are continuous between the lid and the interior, and the surface temperature of the lid is fixed. It is important to note that this lid thickness is not directly equivalent to the lithospheric thickness as defined in [29].

Different runs are characterized by different values of three parameters: the Rayleigh number, Ra, λ and γ, where:

$$Ra = \frac{\rho g \alpha F d^4}{k \kappa \eta}, \quad \lambda = \frac{d_m}{d}, \quad \gamma = \frac{w}{d} \tag{1}$$

g is the acceleration due to gravity; d_m is the conducting lid thickness; d is the thickness and w the width of the convective layer; α is the thermal expansion coefficient; F is the heat flux per unit area into the base of the box; κ is the thermal diffusivity; k is the thermal conductivity; ρ is the density; and η is the dynamic viscosity, which is assumed not to vary with temperature. The aspect ratio γ is 1.5, a typical value from laboratory convection experiments; κ is fixed at $8 \times 10^{-7}\ m^2 s^{-1}$, α at $3.28 \times 10^{-5}\ °K^{-1}$, k at 3.17 $Wm^{-1}\ °K^{-1}$ and ρ at 3300 Mg m^{-3}. The range of parameters explored are: Ra, 6575–1.775×10^7; and λ, 0.0625–0.25. The mesh

spacing varies slightly between runs but is typically 9 km or less.

Runs using different values of Ra and λ produce dimensionless values for temperature, vorticity and stream function which can then be scaled to real values. The scalings used are as follows:

$$r, z = d(r', z') \tag{2}$$

$$t = \frac{d^2 t'}{\kappa} \tag{3}$$

$$u = \frac{\kappa u'}{d} \tag{4}$$

$$T = \frac{Fd}{k} T' \tag{5}$$

where: t is time; T is temperature; r and z are the radial and vertical co-ordinates; u is velocity; and primes refer to dimensionless variables.

In order to obtain dimensioned from dimensionless quantities, the heat flux, F, and the depth of the convecting interior, d, are specified. Since the temperature at the surface, T_s is known, the temperature at the centre of the box, T_c, is then fixed by Eq. (5):

$$T_c = T_s + \frac{Fd(T_c' - T_s')}{k} \tag{6}$$

where T_c' and T_s' are the dimensionless values of temperature at the centre of the plume and at the lid surface, respectively. The viscosity, η, is then also fixed by Eq. (1).

Melting is calculated using the same method as W&M, using a new version of the parameterization for $\Delta S = 330$ J kg^{-1}°C^{-1}:

$$\Delta T = \sum_{m=1}^{2} \sum_{n=0}^{3} a_{mn} \Delta\Theta^m P^n \tag{7}$$

where $a_{10} = 0.5727$, $a_{20} = -0.0001$, $a_{11} = -0.0487$, $a_{12} = -0.0025$, $a_{13} = -0.0001$; $\Delta T = T - T_s(P)$; T is the temperature calculated from decompression melting; $T_s(P)$ is the solidus temperature at that pressure; $\Delta\Theta$ is the potential temperature of the solid prior to melting minus the potential temperature of the solidus at that pressure; P is the pressure; and ΔS is the entropy of melting. The surface deformation and vertical component of the gravity anomaly, g_z, are calculated using the method of Parsons and Daly [30], using an elastic thickness of 30 km appropriate for plume sites [10–12]. The effect of the elastic lid is incorporated by multiplying the bathymetry kernels by a factor dependent on wavelength and elastic thickness, which acts as a low-pass filter ([31], appendix C). The radial component of the gravity anomaly, g_r, is obtained using a method described in Appendix A, and the tangential component of the gravity anomaly, g_ϕ, is zero for the axisymmetric case. The component of the theoretical acceleration (calculated at the altitude of the spacecraft) directed towards Earth can then be compared with the actual line of sight (LOS) acceleration experienced by the Magellan spacecraft by projecting the gravity vector, **g**, onto the line of sight. The theoretical topography does not include any contribution from melt generation.

The admittance is calculated using the method described in [8]: the theoretical gravity and topography profiles are rotated about a vertical axis, and the resultant fields are gridded and can then be transformed as for real data. The admittance is expressed as the value at a wavelength of 1600 km, which is typical of convective processes.

Both gravity and deformation depend mainly on the temperature structure in the upper boundary layer, which is independent of the thickness of the convecting layer for constant heat flux. For this reason, the layer depth is not constrained by the observations.

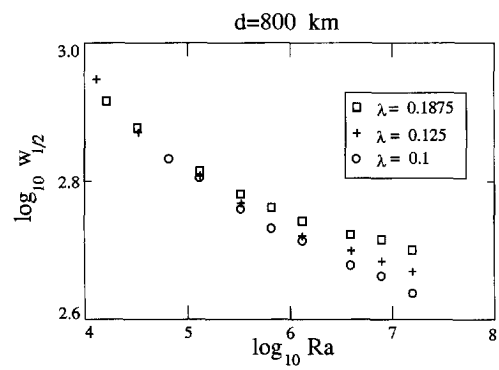

Fig. 1. Full width at half maximum ($w_{1/2}$) for plume gravity profiles produced by convective runs all with a fixed convecting depth (800 km) but varying dimensionless lid thicknesses (λ) and Rayleigh number (Ra), plotted on a log–log scale. Ra varied from 1.32×10^4 to 1.58×10^7.

4. Modelling the observables

In order to reproduce the observables at the three sites chosen, different combinations of Ra and λ are used, with the surface temperature and elastic thickness fixed at 450°C and 30 km respectively, and F and d being varied to obtain a good match. The observables used are the amplitude and width of the gravity and surface topography anomalies, and the variation in LOS acceleration of the Magellan spacecraft.

The spherical harmonic expansion of the gravity field is only known to $l = m = 90$, where l and m are the degree and order, respectively. This means that signals with a wavelength shorter than ~420 km are not present in the field calculated from the spherical harmonics. We wish to compare theoretical

Table 1
Combinations of model parameters producing a plume width of 500 km

Ra		λ			
		0.1	0.125	0.1875	0.25
3.29×10^4	d (km)	525	520	500	–
3.29×10^5	d (km)	665	665	640	615
3.95×10^6	d (km)	870	840	760	695
7.89×10^6	d (km)	910	860	775	705
1.58×10^7	d (km)	950	890	775	705

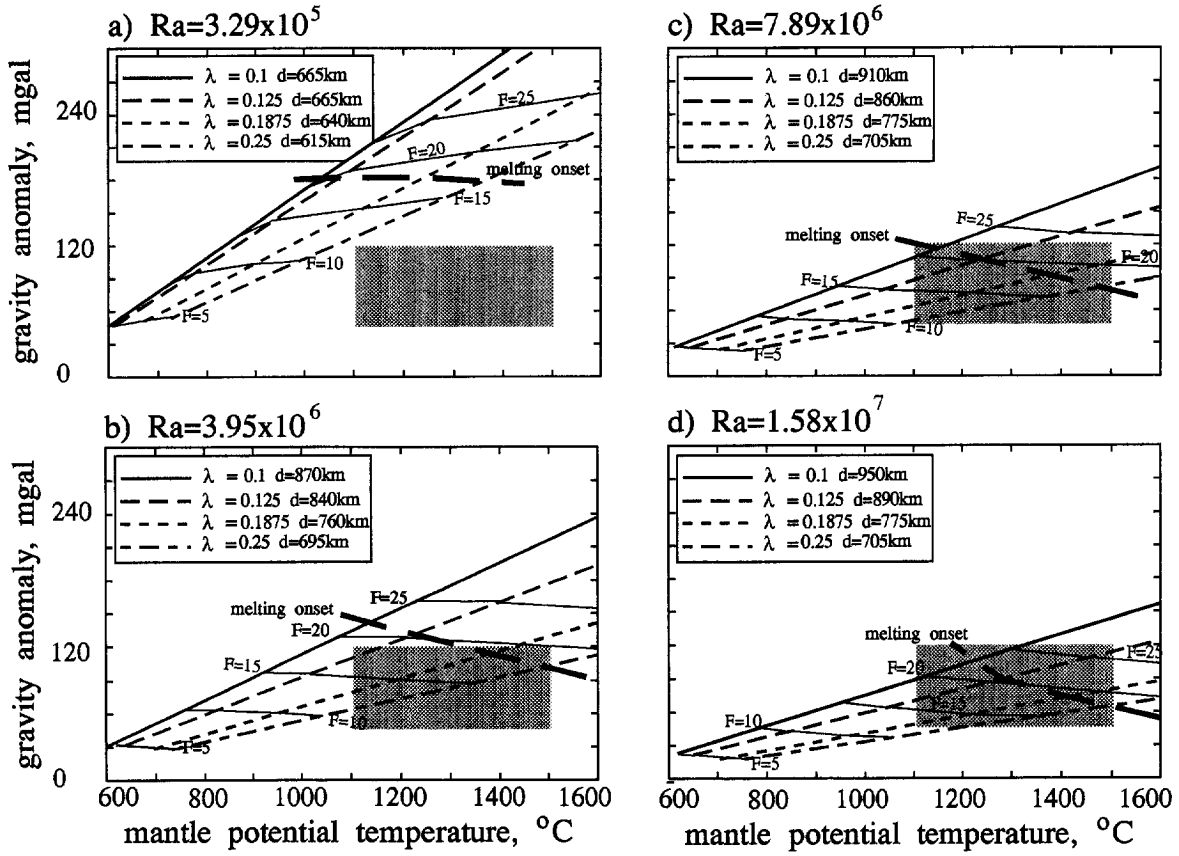

Fig. 2. (a) Peak-to-trough gravity anomaly (evaluated at an altitude of 70 km) and mantle potential temperature for different convection runs, all of which produce a full width at half maximum of 500 km. Bold lines represent one convective model with fixed depth (d), Rayleigh number (Ra) and dimensionless lid thickness (λ) and varying values of heat flux (F, expressed in mW m^{-2}). Thin lines are contours of heat flux. The grey box is the parameter space within which the Hawaii-scale features on Venus are thought to lie. The bold dashed line is the locus of points above which melt production is greater than zero. The Rayleigh number in this case is 3.29×10^5. (b). As (a), except $Ra = 3.95 \times 10^6$. (c). As (a), except $Ra = 7.89 \times 10^6$. (d) As (a), except $Ra = 1.58 \times 10^7$.

profiles of gravity across the model plumes with the observed profiles. Since the observed profiles are obtained from spherical harmonics, these profiles lack short wavelength information contained in the model profiles. We therefore need to low-pass filter the model profiles. A convenient way to do so is to compare the profiles at some height h above the surface. Signals are attenuated by a factor of $\exp(-2\pi h/\lambda)$ where λ is the wavelength, so at 70 km height a signal with wavelength 420 km will be attenuated by a factor of about $1/e$. The gravity field from spherical harmonics is calculated at the same altitude in order to make comparison independent of the height used. The 70 km altitude is arbitrary: using a lower height would increase the amount of short wavelength information present in the model profile but not in the profile from spherical harmonics. The amplitude of the gravity anomaly, Δg, is defined as the peak to trough difference; the width of the anomaly, $w_{1/2}$, is defined as the width of the anomaly at half its maximum height, where the maximum value is measured relative to a gravity anomaly of zero.

Matching gravity rather than topography is used as the main constraint because the topography is affected by rifting and volcanic construction at short wavelengths. The LOS acceleration is used as an additional constraint because it retains shorter wavelength information not present in the spherical harmonic gravity. We compare the modelled and observed LOS accelerations at the average altitude of the spacecraft.

The requirement that $w_{1/2}$ is about 500 km places some constraints on Ra and d. Fig. 1 shows the variation of $w_{1/2}$ with Ra and λ when d is fixed at 800 km. As Ra increases, $w_{1/2}$ decreases, and even at the highest Ra used, differing values of λ have only a small effect on $w_{1/2}$. Similarly, for fixed Ra, $w_{1/2}$ increases proportionately with d but is independent of heat flux. The width of the plume should be controlled by the same factors as the thickness of the thermal boundary layer, δ, which McKenzie et al. [32] show obeys the following relationship:

$$\frac{\delta}{d} \sim Ra^{-1/4} \tag{8}$$

Table 2
Convective models satisfying gravity, width and melt generation constraints

Run	F (mW m^{-2})	T_p (°C)	Ra	λ	d (km)	d_m (km)	ν (m^{2}s^{-1})	Δg (mgal)	Δh (m)	H_r (m^{3}s^{-1})	$Z(k)$ (mgal/km)
V1	20	1210	3.95×10^6	0.1250	840	105	0.29×10^{18}	128	2847	0	49.6
V2	15	1196	3.95×10^6	0.1875	760	143	0.15×10^{18}	91.3	1914	0	51.9
V3	15	1341	3.95×10^6	0.2500	695	174	0.10×10^{18}	86.8	1729	0	53.5
V4	20	1105	7.89×10^6	0.1000	910	91	0.20×10^{18}	109	2585	0	47.5
V5	20	1232	7.89×10^6	0.1250	860	108	0.16×10^{18}	105	2416	0	48.8
V6	15	1219	7.89×10^6	0.1875	775	145	0.79×10^{17}	75.8	1629	0	51.4
V7	18	1373	7.89×10^6	0.1875	775	145	0.94×10^{17}	90.1	1955	0	51.4
V8	19	1424	7.89×10^6	0.1875	775	145	0.10×10^{18}	96.0	2064	1.1	51.4
V9	20	1475	7.89×10^6	0.1875	775	145	0.10×10^{18}	101	2173	5.5	51.4
V10	15	1367	7.89×10^6	0.2500	705	176	0.54×10^{17}	72.0	1467	0	51.9
V11	20	1129	1.58×10^7	0.1000	950	95	0.12×10^{18}	92.1	2217	0	47.4
V12	21	1163	1.58×10^7	0.1000	950	95	0.12×10^{18}	96.7	2328	0	47.4
V13	25	1298	1.58×10^7	0.1000	950	95	0.15×10^{18}	115	2772	9.9	47.4
V14	20	1255	1.58×10^7	0.1250	890	111	0.91×10^{17}	86.7	2023	0	48.0
V15	22	1336	1.58×10^7	0.1250	890	111	0.10×10^{18}	95.3	2225	3.2	48.0
V16	25	1457	1.58×10^7	0.1250	890	111	0.11×10^{18}	108	2529	24.9	48.0
V17	15	1213	1.58×10^7	0.1875	775	145	0.39×10^{17}	57.6	1278	0	50.2
V18	20	1467	1.58×10^7	0.1875	775	145	0.52×10^{17}	76.8	1703	3.2	50.2
V19	21	1518	1.58×10^7	0.1875	775	145	0.55×10^{17}	80.7	1789	12.0	50.2
V20	15	1364	1.58×10^7	0.2500	705	176	0.27×10^{17}	55.3	1157	0	53.2

T_p is the potential temperature at the centre of the plume; ν the kinematic viscosity; H_r the melt generation rate and $Z(k)$ the admittance at 1600 km; all other symbols defined in the text.

However, Fig. 1 demonstrates that the dependence of $w_{1/2}$ on Ra is not as strong as suggested by Eq. (8). Table 1 shows different combinations of Ra, λ and d which produce a full width of 500 km, and demonstrates that a relatively restricted group of models will produce profiles of the correct width.

The amplitude of the gravity and topography anomalies increase with increasing heat flux and d. Parsons and Daly [30] show that:

$$\Delta h \propto \frac{\eta}{d} Ra^{1/2} = \left(\frac{\rho g \alpha F \eta d^2}{k\kappa} \right)^{\frac{1}{2}} \quad (9)$$

Hence increasing the Rayleigh number by reducing viscosity reduces Δh.

Fig. 2 shows the gravity anomaly and mantle potential temperature produced by combinations of F, Ra and d which have a full width of 500 km. The shaded box shows the range of gravity anomalies and likely potential temperature for the entire set of Hawaii-scale plumes, and the dashed line shows the values at which melting first occurs. Since some, but not all, plume sites show volcanic flows it is likely that the plume sites will plot close to the lines depicting onset of melting. Fig. 2a shows that it is difficult to produce plume profiles of the correct

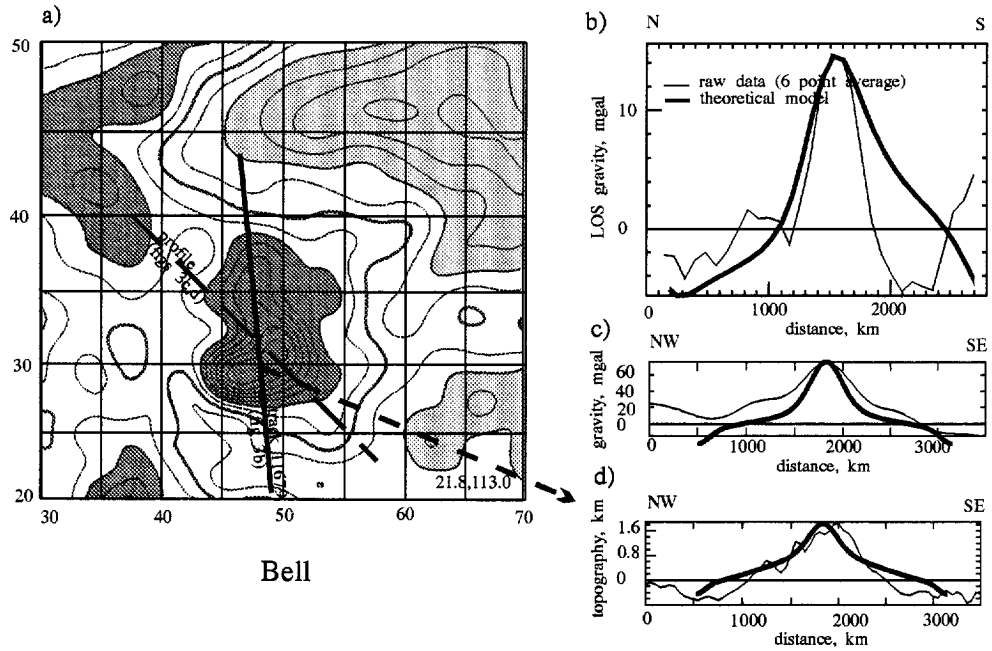

Fig. 3. (a) Contour map of gravity anomaly evaluated at 70 km altitude using the 90th degree and order spherical harmonic field. Contour interval is 10 mgal. The bold contour line is the zero contour; dark shaded areas are above +20 mgal and light shaded areas are below −20 mgal. The continuous bold line labelled 'track 11679' is the segment of that Magellan orbit from which information is depicted in (b). The long dashed bold line is the location of the profile which is shown in (c) and (d). The short dashed bold line with an arrow is pointing in the direction of the Earth at the time of the orbit number. The first number gives the elevation in degrees of the Earth relative to the local horizontal; the second number is the azimuth in degrees measured relative to the local north. (b). The thin continuous line is the total line-of-sight (LOS) acceleration, averaged over 6 points, from the raw Magellan data, orbit number 11679, plotted against distance from the north end of the segment of that orbit (see (a)). The bold line is the theoretical LOS acceleration, evaluated at the average altitude of the spacecraft (197 km), using model V15 (see Table 2) and assuming the plume is centred at 30°N, 48°E. Both profiles have had the average acceleration removed. The variation in altitude of the spacecraft over the orbit segment was 189–212 km. (c) The thin continuous line is the vertical gravity anomaly, evaluated at a height of 70 km from the $l = m = 90$ spherical harmonic gravity field, along the bold dashed line in (a). The starting location of the profile was 40°N, 37.5°E and the line was oriented at 135° to N. The bold continous line is the theoretical gravity profile along the same line from model V15. (d) The thin continuous line is the topography, evaluated along the same line as (c) using the $l = m = 75$ spherical harmonic topography. The bold line is the theoretical topography profile along the same line from model V15.

shape and size for *Ra* much less than 3.95×10^6, unless the lid thickness is a large (> 0.25) fraction of the convecting region, when it is very hard to generate melt. Conversely, for values of *Ra* much greater than 1.58×10^7 it is difficult to produce large enough gravity anomalies unless the lid is very thin, which leads to melt generation rates greater than 0.4. A selection of models plotting within the shaded box are summarized in Table 2.

Both Farida and Bell show large flows overprinting earlier fractures, which suggests that melting has occurred recently. Figs. 3 and 4 show maps of the gravity anomalies around the two plume sites, together with gravity and topography profiles across the plumes and the spacecraft acceleration during one particular pass over each plume. Although different in planform, the two plumes have similar amplitudes and full widths. Also shown are the theoretical profile and acceleration from model V15, which includes a small amount of melting (0.1 km^3 a^{-1}). For Farida the fit is good; for Bell the gravity anomaly is slightly too large but, although the fit is improved by slightly reducing the heat flux or increasing the dimensionless lid thickness (models V14 and V3) this stops any melting. The fit is degraded by the strongly asymmetric planform, also seen in the topographic profile. Phoebe (Fig. 5) has a similar gravity anomaly to Bell but shows fewer signs of recent melting. It is therefore better fit by model V7 which produces no melt. Models V15 and V7 have similar mantle potential temperatures, heat fluxes, viscosities and lid thicknesses. The admittance values for V15 and V7 are 48.0 and 51.4 mgal/km, respectively, which agree well with the value of 50 mgal/km obtained from the global LOS data [8].

The admittance and melt generation are both critically dependent on the thickness of the conductive lid and can therefore be used to constrain this thickness. Over individual plume regions, the admittance at 1500 km is typically 40–60 mgal/km [10–12]. Fig. 6a shows the variation in admittance with conductive lid thickness for a range of models all having a full width of 500 km, and demonstrates that models with lid thicknesses greater than 300 km are unlikely to fall within the range 50 ± 10 mgal/km.

Variations in the lid thickness of models matching

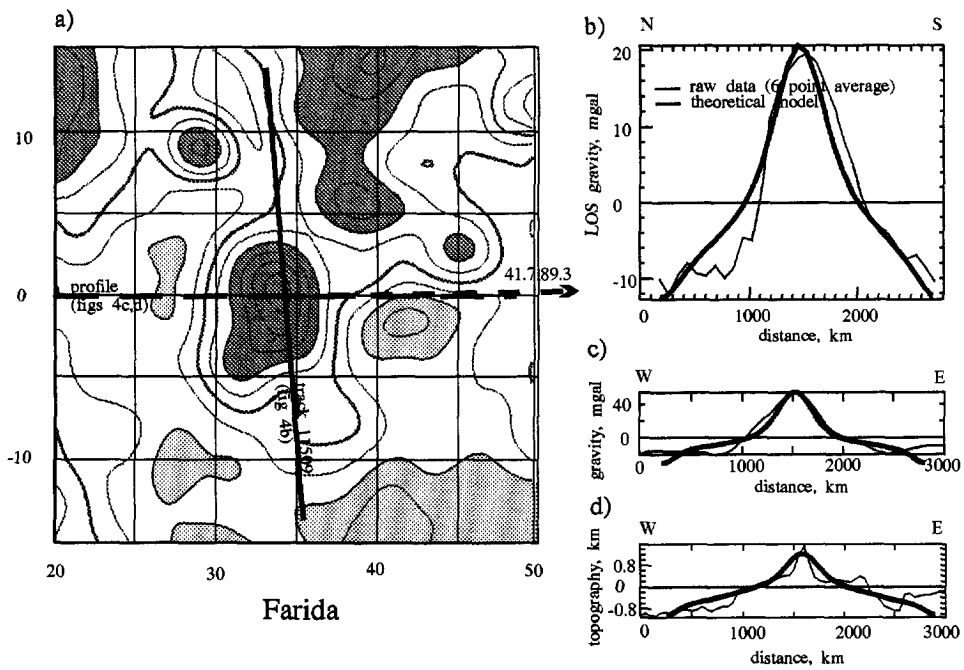

Fig. 4. (a) As Fig. 3a, except the orbit number is 11509. (b) As Fig. 3b, except the theoretical plume (model V15) is centred at 0°N, 34°E and the average altitude is 196 km, varying between 188 and 211 km. (c) As Fig. 3c, except the starting location of the profile was 0°N, 20°E and the profile was oriented at 90° to N. The theoretical profile is from model V15. (d) As Fig. 3d.

the observables may be approximated by adding or subtracting a pressure term to the pressure field in the melting calculations and converting the resultant pressure to lid thickness. As argued above, the maximum melt generation rate is 13 m^3 s^{-1}; the minimum melt generation rate is unknown, but must be greater than zero. Apart from lid thickness, the main control on melt generation rate is mantle potential temperature: no melt will be produced below 1000°C and the mantle potential temperature (T_p) is not greater than 1500 M92. Fig. 6b shows the melt generation rate as a function of lid thickness for a high melt generation (high T_p) and a low melt generation (low T_p) case, both of which have the same width (500 km) and gravity anomaly (95 mgal). Other models having the same width and gravity anomaly plot between these two curves. For any region fitting these criteria in which melt is produced the lid thickness cannot be greater than about 150 km. Areas such as Bell and Farida show no signs of extensive rifting, which suggests that the original lid thickness cannot be greater than 150 km. Similarly, if the lid thickness is less than 20 km too much melt will be produced. Using McKenzie and Bickle's [29] definition of the lithosphere, a conductive lid thickness of about 150 km (models V2 and V19) is equivalent to a lithospheric thickness of 170 km.

Both melt generation and admittance therefore provide a constraint on lid thickness; melt generation is the stronger constraint, limiting the lid thickness to less than 150 km if melting is required to occur.

5. Discussion

Table 2 shows that the set of models fitting the Hawaii-scale features have certain characteristics in common. The lid thickness is probably less than 150 km for a typical Hawaii-scale feature and is constrained by the uncertainty in melt generation and admittance. The Rayleigh number is constrained to be greater than about 4×10^6 by the plume shapes.

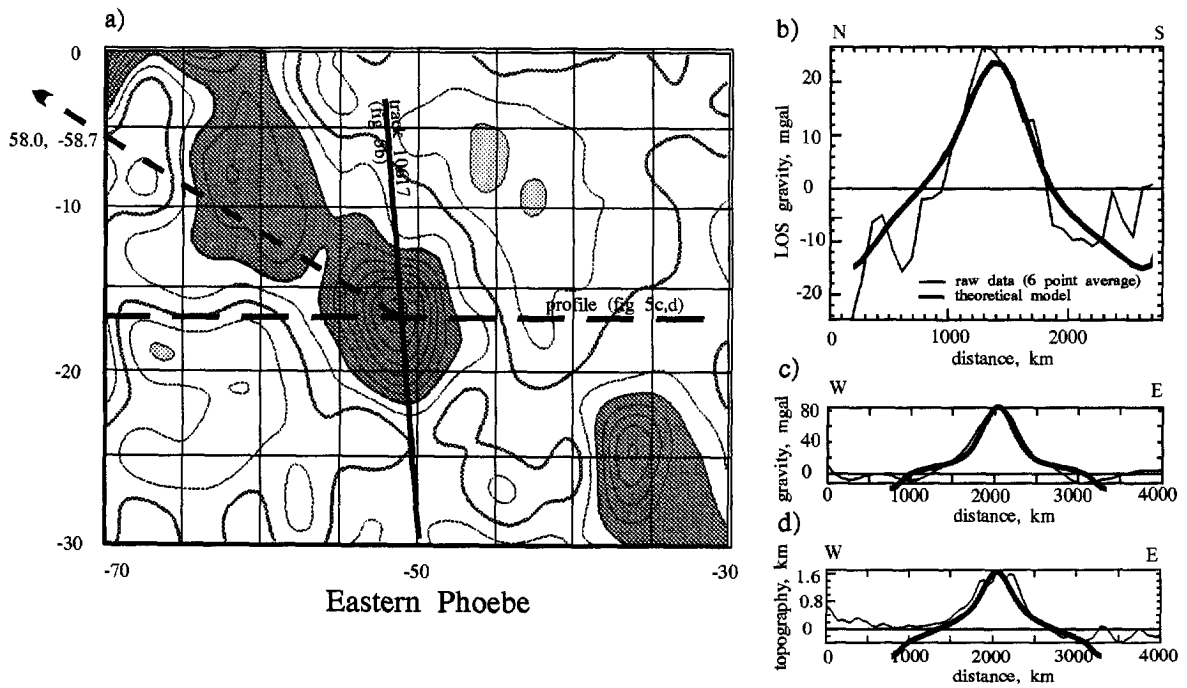

Fig. 5. (a) As Fig. 3a, except the orbit number is 10617. (b) As Fig. 3b, except the theoretical plume (model V7) is centred at 17°S, 51°W and the average altitude is 233 km, varying between 208 and 264 km. (c) As Fig. 3c, except the starting location of the profile was 17°S, 70°W and the profile was oriented at 90° to N. The theoretical profile is from model V7. (d) As Fig. 3d except the theoretical profile is from model V7.

Heat flux varies between 15 and 25 and viscosity between 8.9×10^{19} to 9.6×10^{20} Pa s. Fig. 7 is a summary of model V15, which shows the lid thickness and the melting zone. The radial extent of the melting zone is similar to that of W&M's model for Hawaii, but the Venus plume produces its melt at greater depths and at a slightly lower rate (0.1 km^3 a^{-1} against 0.16 km^3 a^{-1}), although compositions

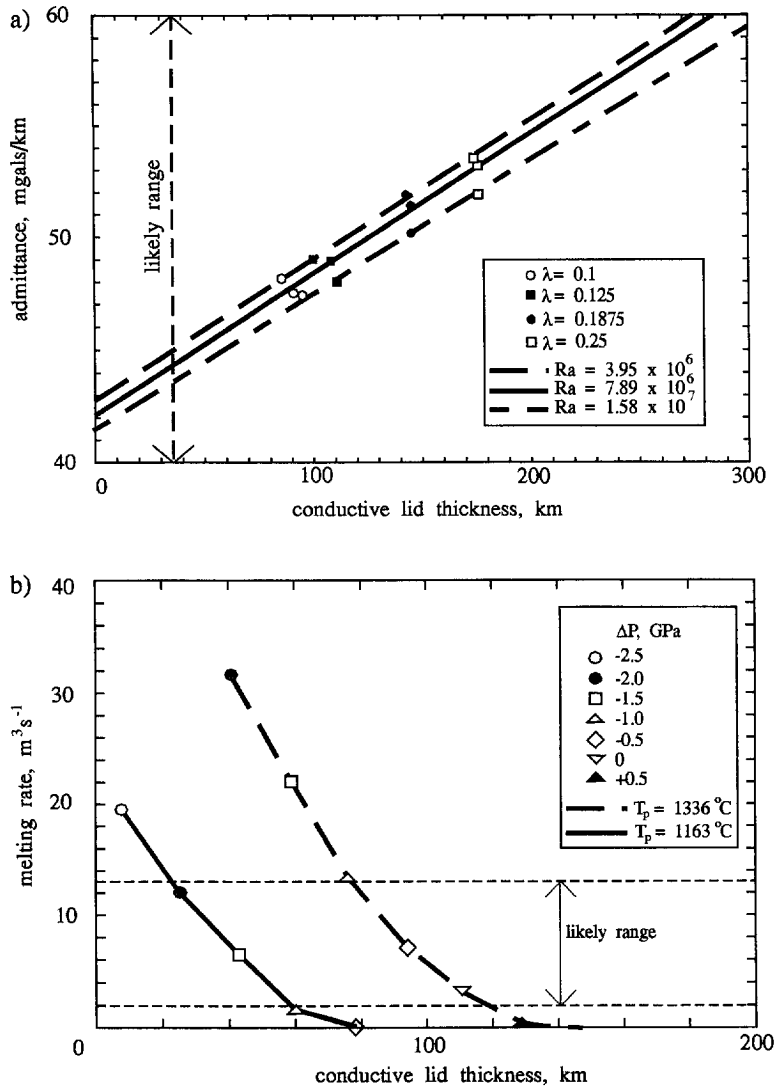

Fig. 6. (a) Admittance of the models in Table 2 plotted against thickness of the conductive lid for different dimensionless lid thickesses (λ) and Rayleigh number (Ra). The three bold lines join points sharing the same value of Ra. The thin dotted line indicates the likely range of admittance for Hawaii-scale plumes on Venus. (b) Melt generation rate plotted against conductive lid thickness for a high potential temperature case (dashed line; model V15 in Table 2) and a low potential temperature case (solid line; model V12). The lid thickness is varied by adding or subtracting a constant pressure (ΔP) to the pressure field for the melting calculations, and then converting the resultant pressure to depth. 1 GPa is approximately 35 km on Venus. The dotted lines indicate the likely range of melt generation rate for Hawaii-scale features. For the high temperature case $Ra = 1.58 \times 10^7$, $T_p = 1336$ and $\eta = 3.2 \times 10^{20}$ Pa s; for the low temperature case $Ra = 1.58 \times 10^7$, $T_p = 1163$ and $\eta = 4.2 \times 10^{20}$ Pa s. η is the viscosity, Ra the Rayleigh number and T_p the potential temperature of the centre of the convecting region.

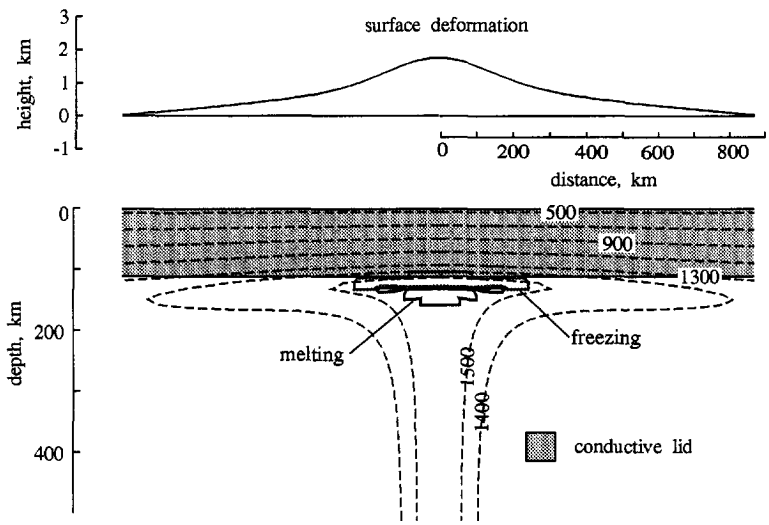

Fig. 7. Summary diagram of model V15 showing the region of melting and the surface deformation associated with the convection. Melt generation occurs in the region in which the instantaneous melt production rate > 0; melt freezing occurs where the instantaneous melt production rate < 0 (see [28] for more details). Dashed lines are temperature contours in degrees C. The depth of the convective layer is not well determined (see text).

Table 3
Comparison of best-fitting Venus model with Hawaii and measured Venusian surface compositions

	Units	V15	Hawaii	Venera 13	Venera 14	Vega 2
F	mW m^{-2}	22	51			
T_p	°C	1336	1280			
Ra		1.58×10^7	1.78×10^7			
λ		0.125	0.179			
d	km	890	401			
d_m	km	111	72			
η	Pa s	3.3×10^{20}	3.0×10^{19}			
Δg	mgal	95	70			
Δh	km	2.2	1.3			
H_r	km^3 a^{-1}	0.1	0.16			
H_v	m^3	1.3×10^{15}	5.5×10^{14}			
T_m	°C	1223	1154			
$T_{30\,km}$	°C	658	480			
T ($plume$)	°C	1600	1560			
SiO_2	wt%	49.7	48.3	45.1 ± 3.0	48.7 ± 3.6	45.6 ± 3.2
TiO_2	wt%	1.49	1.12	1.59 ± 0.45	1.25 ± 0.41	0.2 ± 0.1
Al_2O_3	wt%	10.7	11.7	15.8 ± 3.0	17.9 ± 2.6	16 ± 1.8
FeO	wt%	12.3	11.7	9.3 ± 2.2	8.8 ± 1.8	7.7 ± 1.1
MgO	wt%	15.2	15.6	11.4 ± 6.2	8.1 ± 3.3	11.5 ± 3.7
CaO	wt%	8.1	7.33	7.1 ± 1.0	10.3 ± 1.2	7.5 ± 0.7
Na_2O	wt%	2.02	1.88	–	–	–
K_2O	wt%	0.20	0.21	4.0 ± 0.63	0.2 ± 0.07	0.1 ± 0.08

T_p is the potential temperature at the centre of the plume; $T(plume)$ the maximum potential temperature of the plume; H_r is the melt generation rate; H_v the volume of mantle involved in melting; T_m the temperature at the base of the conducting lid; and $T_{30\,km}$ the tempeature at 30 km depth. All other notation defined in the text. The model compositions are derived using the parameterization of Watson and McKenzie, Appendix C [28] and the compositions for the Venera and Vega landers are from [27], table 2.

are very similar. Table 3 summarizes the contrasts between model V15, W&M's Hawaii model and the surface compositions recorded by the Soviet landers. Since FeO melt concentrations depend almost entirely on mantle potential temperature (W&M, Table 2), lower FeO concentrations for the Vega and Venera samples suggest that these compositions were produced by melting at lower temperatures than those in the two model plumes.

The elastic thickness of terrestrial oceanic lithosphere follows an isotherm between 450°C and 600°C [9]. The homologous temperature is defined as the ratio of the current temperature (in K) to the solidus temperature, which for wet (0.2% H_2O) mantle at 1 GPa is about 1050°C [33]. The corresponding homologous temperature range is 0.55–0.66; for dry mantle material this is equivalent to a temperature of 590–763°C. The homologous temperature is critical in determining the behaviour of materials (e.g. [34]). Since Venus is dry, we might expect the elastic thickness to be determined by the depth to this latter temperature range. If the elastic thickness for Venus is determined by the 675°C isotherm, the models in Table 2 would have elastic thicknesses between 27 km and 48 km. These values are similar to other estimates of t_e over plume sites [8,10–12].

The thickness of the mechanical boundary layer from these studies is at most twice that estimated by W&M for Hawaii, and is significantly smaller than some other models of convection on Venus [11,35,36]. However, the requirements for an internal temperature similar to that of the Earth and a modest amount of melting do appear to constrain the conductive lid thickness to be at most 150 km, given the assumptions of the model. A similar conclusion is reached by Smrekar and Parmentier [37]. On the basis of the admittance data alone the lid thickness is unlikely to be greater than 300 km.

Under conditions of temperature-dependent viscosity, convection produces a thick, stagnant lid in which most of the viscosity variation occurs, with a nearly isothermal (and hence isoviscous) core beneath [36,38]. Lateral variations in viscosity will exist below the stagnant lid, but Moresi and Parsons [39] show that the horizontal average of viscosity gives a good approximation to the long wavelength behaviour of the surface observables, even for a steady-state model. Modelling the temperature-dependent case as a rigid lid overlain by an isoviscous fluid is therefore probably a reasonable approximation.

W&M estimated η beneath Hawaii to be 3×10^{19} Pa s. The values obtained in this study of around 3×10^{20} Pa s suggest that Venus lacks a low viscosity layer, in agreement with other studies [4,36,40]. A high upper mantle viscosity would cause a large drag force to be exerted on any moving plate, perhaps helping to explain the apparent absence of large-scale plate motions on Venus at the present day. The reason for the lack of a low viscosity zone may be associated with the fact that the mantle on Venus is probably drier than that on Earth, and therefore less likely to melt.

One obvious conclusion from the SAR images is that many of the sites of large-scale melt generation are not now associated with positive gravity anomalies nor, presumably, plumes. This implies that the convective planform is time-dependent on a timescale small compared to the interval since the last resurfacing event ($\sim$ 500 Ma). On the other hand, some possible plume sites (e.g. that at 26°N, 178°E) show no signs of melting at all. One way of initiating melting is by rifting: although model V7 produces no melt, thinning the lid by 30% over the plume is enough to initiate melt production.

The SAR images also reveal that some of the Hawaii-scale plume sites with smaller gravity anomalies (e.g. those at 8°S, 138°W and 16°S, 117°W) are the sites of coronae. These observations imply that coronae may be at least partly convective in origin, as other authors have also suggested (e.g. [41]).

The model assumes that the plumes are maintained by heating from below but does not place any constraints on the depth to which convection occurs. The assumption that heating is from below implies that the upper mantle convects independently of the lower mantle; it is still unclear as to whether this is actually the case for Venus or the Earth. The low value of the surface heat flux (assuming no internal heating in the convecting layer) agrees with other studies [36,37]. The value obtained is about one third the value of the calculated heat production rate compared with Earth, where the heat loss is approximately twice the heat production rate. This strongly suggests that heat loss and heat production do not

have to remain in equilibrium during planetary thermal evolution.

The other main question which remains to be settled is that, since a consistent model can be developed for the Hawaii-scale plumes, how does one model the larger features such as Beta? Since the mantle is convecting at a high Rayleigh number, larger features should exhibit 3D time-dependent behaviour which is not susceptible to axisymmetric steady-state modelling. It may also be important to include the effect of temperature-dependent viscosity, and the influence of melting on viscosity.

Acknowledgements

We thank Jim Alexopoulos and Bill Sjogren for providing us with the orbital data, and Roger Phillips, Sue Smrekar and an anonymous reviewer for greatly improving the paper. Financial support for this work was provided by Shell International Petroleum Company (Studentship to FN), The Royal Society and NERC (grant GR3/08534). *[UC]*

Appendix A

We need the radial component of the gravity field, g_r, given that the vertical component of the gravity field, g_z has been calculated for an axisymmetric plume using the method of Courtney and White [31].

Following their method, the geoid, $N(r)$ and the Hankel transform of the geoid, $\hat{N}(k)$, are related by:

$$N(r) = \int_0^\infty J_0(kr)\,\hat{N}(k)\,k\,\mathrm{d}k \tag{10}$$

The geoid is related to the gravitational potential, $V(r)$ by:

$$V(r) = g_0 N(r) \tag{11}$$

where g_0 is the average vertical gravitational acceleration. In order to find g_r we need $\partial V/\partial r$:

$$g_r = \frac{\partial V(r)}{\partial r} = g_0 \int_0^\infty \frac{\partial J_0(kr)}{\partial r}\hat{N}(k)\,k\,\mathrm{d}k \tag{12}$$

Since:

$$J_0'(z) = -J_1(z) \tag{13}$$

$$g_r = -g_0 \int_0^\infty J_1(kr)\left(k\hat{N}(k)\right)k\,\mathrm{d}k \tag{14}$$

The radial component of the gravity field, g_r, can therefore be calculated from the first-order Hankel transform of $k\hat{N}(k)$. Using the notation of Oppenheim et al. [42]:

$$G(r) = \int_0^\infty J_n(kr)\,g(k)\,k\,\mathrm{d}k \tag{15}$$

can be rewritten as:

$$G(r) = \frac{i^{(-n)}}{2\pi}\int_{-\infty}^{\infty} e^{irx}p(x)\,\mathrm{d}x \tag{16}$$

where $p(x)$ is the weighting function:

$$p(x) = 2\int_x^\infty g(k)\frac{k}{\left(k^2-x^2\right)^{1/2}}T_n(x/k)\,\mathrm{d}k \tag{17}$$

and T_n is the nth order Chebyshev polynomial. We need the expression for $n = 1$, when:

$$T_1(x/k) = \frac{x}{k} \tag{18}$$

and:

$$p(x) = 2x\int_x^\infty \frac{g(k)}{\left(k^2-x^2\right)^{1/2}}\mathrm{d}k \tag{19}$$

If $g(k)$ is a piecewise continuous function sampled at an interval δk and $g(k)$ is zero for $k > N\delta k$ then:

$$p(x) = 2x\sum_{j=m}^{N} g(j\delta k)\int_{k_1}^{k_2}\frac{1}{\left(k^2-x^2\right)^{1/2}}\mathrm{d}k \tag{20}$$

where $x = m\delta k$, $k_1 = j\delta k - (\delta k/2)$ and $k_2 = j\delta k + (\delta k/2)$. This reduces to:

$$p(x) = 2x\sum_{j=m}^{N} g(j\delta k)\left(\cosh^{-1}(k_2/x) - \cosh^{-1}(k_1/x)\right) \tag{21}$$

Once $p(x)$ has been obtained, g_r can then be obtained by use of Eq. (17):

$$g_r = -\frac{g_0}{2\pi i}\int_{-\infty}^{\infty} e^{irx} p(x)\,\mathrm{d}x \qquad (22)$$

which is simply a Fourier transform.

References

[1] R.S. White and D.P. McKenzie, Mantle plumes and flood basalts, J. Geophys. Res. 100, 17543–17585, 1995.

[2] G.E. McGill, J.L. Warner, S.J. Steenstrup, C. Barton and P.G. Ford, Continental rifting and the origin of Beta Regio, Venus, Geophys. Res. Lett. 8, 737–740, 1981.

[3] R.J. Phillips and M.C. Malin, The interior of Venus and tectonic implications, in: Venus, D.M. Hunten, L. Colin, T.M. Donahue and V.I. Moroz, eds., pp. 159–214, Univ. of Arizona Press, Tucson, 1983.

[4] R.J. Phillips, Convection-driven tectonics on Venus, J. Geophys. Res. 95, 1301–1316, 1990.

[5] S.E. Smrekar and R.J. Phillips, Venusian highlands — geoid to topography ratios and their implications, Earth. Planet. Sci. Lett. 107, 582–597, 1991.

[6] D.L. Bindschadler, G. Schubert and W.M. Kaula, Coldspots and hotspots: global tectonics and mantle dynamics of Venus, J. Geophys. Res. 97, 13495–13532, 1992.

[7] E.R. Stofan, S.E. Smrekar, D.L. Bindschadler and D. Senske, Large topographic rises on Venus: implications for mantle upwelling, J. Geophys. Res. 100, 23317–23327, 1995.

[8] D. McKenzie, The relationship between topography and gravity on Earth and Venus, Icarus 112, 55–88, 1994.

[9] A.B. Watts and S.F. Daly, Long wavelength gravity and topography anomalies, Annu. Rev. Earth. Planet. Sci. 9, 415–458, 1981.

[10] S.E. Smrekar, Evidence for active hotspots on Venus from analysis of Magellan gravity data, Icarus 112, 2–26, 1994.

[11] R.J. Phillips, Estimating lithospheric properties at Atla Regio, Venus, Icarus 112, 147–170, 1994.

[12] D. McKenzie and F. Nimmo, Elastic thickness estimates for Venus from line of sight accelerations, Icarus, submitted, 1995.

[13] D.T. Sandwell and G. Schubert, Flexural ridges, trenches and outer rises around coronae on Venus, J. Geophys. Res. 97, 16069–16083, 1992.

[14] C.L. Johnson and D.T. Sandwell, Lithospheric flexure on Venus, Geophys. J. Int. 119, 627–647, 1994.

[15] R.R. Herrick and R.J. Phillips, Geological correlations with the interior density structure of Venus, J. Geophys. Res. 97, 16017–16034, 1992.

[16] B.A. Campbell, Bell Regio, Venus — integration of remote sensing data and terrestrial analogs for geologic analysis, J. Geophys. Res. 99, 21153–21171, 1994.

[17] D. McKenzie, P.G. Ford, C. Johnson, B. Parsons, D. Sandwell, S. Saunders and S.C Solomon, Features on Venus generated by plate boundary processes, J. Geophys. Res. 97, 13533–13544.

[18] G.G. Schaber, R.G. Strom, H.J. Moore, L.A. Soderblom, R.L. Kirk, D.J. Chadwick, D.D. Dawson, L.R. Gaddis, J.M. Boyce and J. Russell, Geology and distribution of impact craters on Venus: what are they telling us? J. Geophys. Res. 97, 13257–13301, 1992.

[19] R.G. Strom, G.G. Schaber and D.D. Dawson, The global resurfacing of Venus, J. Geophys. Res. 99, 10899–10926, 1994.

[20] R.J. Phillips, R.F. Raubertas, R.E. Arvidson, I.C. Sarkar, R.R. Herrick, N. Izenberg and R.E. Grimm, Impact craters and Venus resurfacing history, J. Geophys. Res. 97, 15923–15948, 1992.

[21] N. Namiki and S.C. Solomon, Impact crater densities on volcanoes and coronae on Venus: implications for volcanic resurfacing, Science 265, 929–933, 1994.

[22] R.R. Herrick and R.J. Phillips, Implications of a global survey of Venusian impact craters, Icarus 111, 387–416, 1994.

[23] R.G. Strom, G.G. Schaber, D.D. Dawson and R.L. Kirk, Reply to comment on "the global resurfacing of Venus" by R.G. Strom, G.G. Schaber and D.D. Dawson, J. Geophys. Res. 100, 23361–23365, 1995.

[24] D.W. Caress, M.K. McNutt, R.S. Detrick and J.C. Mutter, Seismic imaging of hotspot-related crustal underplating beneath the Marquesas Islands, Nature 373, 600–603, 1995.

[25] S.C. Solomon and J.W. Head, Mechanisms for lithospheric heat transport on Venus: implications for tectonic style and volcanism, J. Geophys. Res. 87, 9236–9246, 1982.

[26] R.K. O'Nions, S.R. Carter, N.M. Evensen and P.J. Hamilton, Upper mantle geochemistry, in: The Sea, Vol. 7, C. Emiliani ed., Wiley-Interscience, New York, 1981.

[27] A.T. Basilevsky, O.V. Nikolaeva and C.M. Weitz, Geology of the Venera 8 landing site region from Magellan data: morphological and geochemical considerations, J. Geophys. Res. 97, 16315–16336, 1992.

[28] S. Watson and D. McKenzie, Melt generation by plumes: a study of Hawaiian Volcanism, J. Petrol. 32, 501–537, 1991.

[29] D. McKenzie and M.J. Bickle, The volume and composition of melt generated by extension of the lithosphere, J. Petrol. 29, 625–679, 1988.

[30] B. Parsons and S. Daly, The relationship between surface topography, gravity anomalies and temperature structure of convection, J. Geophys. Res. 88, 1129–1144, 1983.

[31] R.C. Courtney and R.S. White, Anomalous heat flow and geoid across the Cape Verde Rise: evidence for dynamic support from a thermal plume in the mantle, Geophys. J. R. Astron. Soc. 87, 815–867, 1986.

[32] D. McKenzie, J.M. Roberts and N.O. Weiss, Convection in the earth's mantle: towards a numerical simulation, J. Fluid Mech. 62, 465–538, 1974.

[33] D.H. Green, Experimental melting studies on a model upper mantle composition at high pressure under water-saturated and water-undersaturated conditions, Earth Planet. Sci. Lett. 19, 37–53, 1973.

[34] S.R. Borch and H.W. Green, Dependence of creep in olivine on homologous temperature and its implications for flow in the mantle, Nature 330, 345–348, 1987.
[35] D.L. Turcotte, An episodic hypothesis for Venusian tectonics, J. Geophys. Res. 98, 17061–17068, 1993.
[36] V.S. Solomatov and L.N. Moresi, Stagnant lid convection on Venus, J. Geophys. Res. 101, 4737–4753, 1996.
[37] S.E. Smrekar and E.M. Parmentier, The interaction of mantle plumes with surface thermal and chemical boundary layers: applications to hotspots on Venus, J. Geophys. Res. 101, 5397–5410, 1996.
[38] D.B. White, Experiments with convection in a variable viscosity fluid, Ph.D. Thesis, Univ. Cambridge.
[39] L. Moresi and B. Parsons, Interpreting gravity, geoid and topography for convection with temperature dependent viscosity: application to surface features on Venus, J. Geophys. Res. 100, 21155–21171, 1995.
[40] W.S. Kiefer and B.H. Hager, A mantle plume model for the equatorial highlands of Venus, J. Geophys. Res. 96, 20947–20966, 1991.
[41] S.W. Squyres, D.M. Janes, G. Baer, D.L. Bindschadler, G. Schubert, V.L. Sharpton and E.R Stofan, The morphology and evolution of coronae on Venus, J. Geophys. Res. 97, 13611–13634, 1992.
[42] A.V. Oppenheim, G.V. Frisk and D.R. Martinez, An algorithm for the numerical evaluation of the Hankel transform, Proc. IEEE 66, 264–265, 1978.